



# A novel method for the determination of the EEG individual alpha frequency

A. Goljahani <sup>a</sup>, C. D'Avanzo <sup>a</sup>, S. Schiff <sup>b</sup>, P. Amodio <sup>b</sup>, P. Bisiacchi <sup>c</sup>, G. Sparacino <sup>a,\*</sup>

<sup>a</sup> Department of Information Engineering, University of Padova, Italy

<sup>b</sup> Department of Clinical and Experimental Medicine, University of Padova, Italy

<sup>c</sup> Department of General Psychology, University of Padova, Italy

## ARTICLE INFO

### Article history:

Received 3 July 2011

Revised 24 November 2011

Accepted 2 December 2011

Available online 10 December 2011

### Keywords:

Alpha reactivity

Inter-individual variability

Leads selection

Peak frequency

Transition frequency

Spectrum

## ABSTRACT

The individual alpha frequency (IAF) is one of the most common tools used to study the variability of EEG rhythms among subjects. Several approaches have been proposed in the literature for IAF determination, including the popular peak frequency (PF) method, the extended band (EB) method, and the transition frequency (TF) method. However, literature techniques for IAF determination are over-reliant on the presence of peaks in the EEG spectrum and are based on qualitative criteria that require visual inspection of every individual EEG spectrum, a task that can be time consuming and difficult to reproduce. In this paper a novel *channel reactivity based* (CRB) method is proposed for IAF computation. The CRB method is based on quantitative indexes and criteria and relies on task-specific alpha *reactivity* patterns rather than on the presence of peaks in the EEG spectrum. Application of the technique to EEG signals recorded from 19 subjects during a cognitive task demonstrates the effectiveness of the CRB method and its capability to overcome the limits of PF, EB, and TF approaches.

© 2011 Elsevier Inc. All rights reserved.

## 1. Introduction

Since the first EEG recording (Berger, 1929), evidence that particular mental activities or states are reflected by EEG rhythmic patterns at specific frequencies has led to the introduction of the conventional and widely utilised frequency intervals (bands): delta ( $\delta$ , 0.1–3.5 Hz), theta ( $\theta$ , 4–7.5 Hz), alpha ( $\alpha$ , 8–13 Hz), beta ( $\beta$ , 14–30 Hz), and gamma ( $\gamma$ , >30 Hz); see Niedermeyer (2005) and Sanei and Chambers (2007) for reviews. Depending on the inter-individual differences, EEG rhythms can differ in their frequencies from subject to subject (Başar et al., 1997; Klimesch et al., 2000; Niedermeyer, 2005). Since the early attempts to capture these individual features of EEG rhythms and correlate them with individual behavioural states and cognitive traits, the speed of alpha oscillations, the so-called alpha frequency, has turned out to be a meaningful index of inter-individual variability (Başar et al., 1997; Doppelmayr et al., 1998; Hadley, 1941; Klimesch et al., 1993; Klimesch, 1999; Knott, 1938; Niedermeyer, 2005; Osaka, 1984; Pfurtscheller and Lopes da Silva, 1999). In the following we will discuss the most well-known approaches to investigation of the alpha frequency at the individual level and some open issues which motivate the development of a new method.

### 1.1. Literature methods for individual alpha frequency (IAF) determination and margins for improvement

#### 1.1.1. The peak frequency (PF) method

It is well-known that the alpha rhythm is clearly seen under conditions of physical relaxation and relative mental inactivity (IFSECN, 1974). In fact, at resting conditions, the EEG spectrum usually shows a visible peak in the alpha range. Historically, the first method proposed to characterise the individual alpha frequency (IAF) is the so-called peak frequency (PF) method, which consists of localising the frequency  $f_p$  at which this peak occurs. As an example, panel (a) of Fig. 1 shows a representative EEG spectrum at rest, with  $f_p$  represented as a vertical solid line and the alpha range highlighted by two vertical dotted lines.

The PF method has been widely applied in several studies, for instance to show that the mean alpha frequency is  $10.2 \pm 0.9$  Hz in an adult (Petersén and Eeg-Olofsson, 1971), increases from childhood to puberty (Epstein, 1980) and decreases for the rest of the lifespan (Köpruner et al., 1984; Saletu and Grünberger, 1985), is related to head size (Nunez et al., 1978), is lower in demented subjects compared to age matched normal subjects (Coben et al., 1985), predicts age-related decline in working memory (Clarka et al., 2004), is influenced by genetic factors (Smit et al., 2006), and correlates with the amplitude of visual evoked potential and haemodynamic response (Koch et al., 2008). Besides being directly investigated, the frequency  $f_p$  has also been utilised as an anchor point to determine the frequency intervals corresponding to theta and alpha bands (Babiloni et al., 2004, 2010; Capotosto et al., 2009; Doppelmayr et al., 2005; Klimesch et al., 2004).

\* Corresponding author at: Department of Information Engineering, via Gradenigo 6/B, 35131 Padova, Italy. Fax: +39 049 8277699.

E-mail address: [giovanni.sparacino@dei.unipd.it](mailto:giovanni.sparacino@dei.unipd.it) (G. Sparacino).

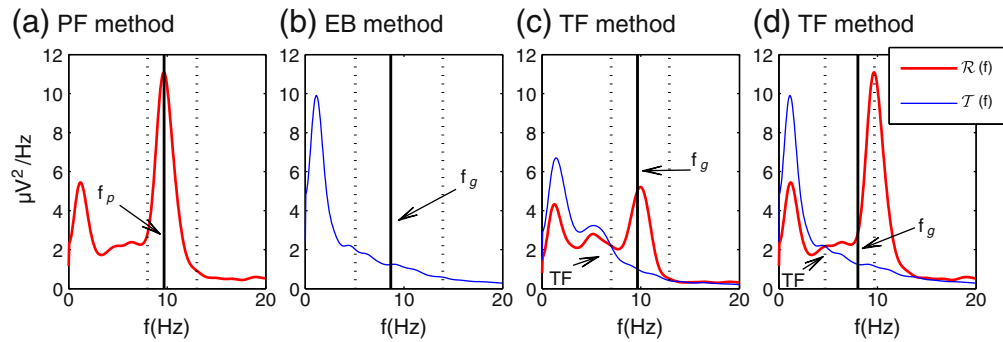


**Fig. 1.** Representative cases of resting (red) and test (blue) EEG spectra. Panel (a) illustrates an example of peak frequency (PF)  $f_p$  determination by the PF method. In the picture, two vertical dotted black lines delimit the (8, 13) Hz alpha range and the vertical solid line is drawn in correspondence with  $f_p$ . Panel (b) shows an example of gravity frequency  $f_g$  determined by the extended band (EB) method for a representative test spectrum that is quite flat in the alpha range. In the picture, a vertical solid line is drawn in correspondence with  $f_g$  and the interval on which it was computed (the extended alpha band) is delimited by two vertical dotted lines. Panels (c) and (d) show two examples of gravity frequencies  $f_g$  determined by the transition frequency (TF) method. The panels depict two representative cases of superimposed resting and test spectra with the relative TFs. For both images, vertical dotted lines delimit the interval from TF to TF + 5 Hz and the vertical solid line is drawn in correspondence with  $f_g$ . (For interpretation of the references to colour in this figure legend, the reader is referred to the web version of this article.)

### 1.1.2. The centre of gravity frequency concept

Drawbacks of the PF method comprise the fact that the definition of  $f_p$  does not cope with cases such as EEG spectra with multiple peaks or EEG spectra that are quite flat in the alpha range. In these cases, which are common when the EEG spectrum is not relative to the resting condition, a more appropriate approach is the one that employs the centre of gravity frequency, that is, the weighted sum of spectral estimates divided by the total alpha power (Klimesch, 1999). This quantity reflects the central tendency of the alpha power and is therefore more representative of the average activity of the alpha population. The determination of the gravity frequency requires the definition of the interval on which the gravity centre will be computed. However, when the EEG spectrum shows multiple peaks or is quite flat, the definition of such an interval is not trivial and deserves further development.

### 1.1.3. The extended band (EB) method

A method that utilises the extended alpha band to compute the gravity frequency, concisely denoted as the extended band (EB) method, was introduced by Klimesch et al. (1990). The procedure can be summarised as follows. First, by visually inspecting each individual EEG recording, subjects without a clearly detectable alpha peak in the resting spectrum are discarded. Then, for each of the remaining subjects, an extended alpha band is determined as follows. First, leads with an evident peak in the alpha interval of the EEG spectrum at rest are selected on a qualitative basis by visual inspection. Then, for each of these leads the frequency interval ( $f_1, f_2$ ) is determined by localising, by visual inspection, the starting point of the ascending edge,  $f_1$ , and the ending point of the descending edge of the alpha peak,  $f_2$ . Finally, the extended alpha band for the subject is obtained by averaging the boundaries of these intervals. Klimesch et al. (1990) called the IAF the frequency that is obtained by utilising the extended alpha band to compute, for each selected lead, the gravity centre of the EEG spectrum relative to the temporal interval under investigation. Either the resting interval or an interval in which the subject is performing the task (test interval) can be utilised. As an example, panel (b) of Fig. 1 shows a representative EEG spectrum computed during a test interval. In the graph, the IAF, denoted by  $f_g$  and computed as the gravity frequency over the extended alpha band delimited by the two vertical dotted lines, is represented as a solid vertical line. The computation of the average IAF over all of the selected leads yields a single frequency for each subject.

Since its first definition, the term “IAF” has been utilised to also denote this average and later any alpha frequency computed on an individual basis. Several results have been published on the relationship

between IAF and memory performance. In particular, Klimesch et al. (1990) found that good memory performers have an IAF about 1 Hz higher than bad memory performers, and hypothesised that this result was an indicator of faster retrieval of information from memory (Klimesch, 1997). IAF has also been utilised as an anchor point to determine the alpha and theta bands as frequency intervals with a fixed (Klimesch, 1997) or percentage (Doppelmayr et al., 1998) width.

The EB method for the IAF determination has some open issues. For instance, when the computation of the IAF is relative to a test interval, the gravity centre of the EEG spectrum is computed over a frequency band that is obtained by exploiting the resting spectra dynamics. This could prevent the capture of the alpha rhythms that are in reality modulated by the mental process relative to the task. Moreover, discarding data relative to subjects with spectra that do not show a clear alpha peak could result in a loss of information about broader aspects of the phenomenon under investigation. Finally, the need for visual inspection of every individual EEG spectrum and the lack of a proper formalisation to assess the presence of peaks in the spectra can make the results difficult to reproduce.

### 1.1.4. The transition frequency (TF) method

Another method for IAF computation was reported by Klimesch (1999). The approach is based on the crucial finding that in most cases when the task demand increases theta synchronises whereas alpha desynchronises (Capotosto et al., 2009; Doppelmayr et al., 1998; Gevins et al., 1997; Grabner et al., 2007; Klimesch et al., 1997; Klimesch, 1999; Lopes da Silva, 1992; Raghavachari et al., 2001; Rugg and Dickens, 1982; Schacter, 1977). In other words, theta power increases (synchronises) during a test interval with respect to a resting interval, whereas the alpha power decreases (desynchronises). As a consequence of this pattern, by superimposing the resting and test spectra, it can be seen that there is a frequency at which the two spectra intersect and the theta synchronisation gives way to alpha desynchronisation. This frequency is defined as the transition frequency (TF) (Klimesch et al., 1996; Klimesch, 1999) and is shown in panel (c) of Fig. 1, where representative resting (red) and test (blue) EEG spectra are reported. TF marks the transition between the alpha and theta bands. Accordingly, the IAF is defined as the peak or gravity frequency of the spectrum over the individual interval ( $f_1, f_2$ ) in which  $f_1$  corresponds to TF, and  $f_2$  is set on an empirical basis (Klimesch, 1999). For instance, a reasonable value for  $f_2$  was suggested to be TF + 5 Hz. In Fig. 1(c) the interval ( $f_1, f_2$ ), determined as suggested above, is shown by two dotted vertical lines. In the same picture, the IAF, determined as the gravity frequency of the interval and denoted as  $f_g$ , is represented as a solid vertical line. The

fundamental novelty of the method using the TF concept, concisely termed the TF method, is the fact that the individualisation of the alpha frequencies is accomplished by exploiting the reactivity of rhythms, rather than by simply utilising the EEG resting spectrum dynamics. In fact, the theta-synchronisation/alpha-desynchronisation pattern is representative of how specific frequencies react to certain stimuli or mental activity. The principle of looking at EEG rhythms' responsiveness is also considered to be fundamental in assessing the normality of an adult EEG (Niedermeyer, 2005). However, a possible drawback of the TF method is the lack of a clear criterion for setting  $f_2$ . In fact, if, for instance, the width of the interval from  $f_1$  to  $f_2$  is set at 5 Hz, some of the frequencies with an alpha desynchronising behaviour could be excluded from the interval, as shown in panel (d) of Fig. 1. As the picture shows, the interval from  $f_1$  to  $f_2$  Hz, delimited by two vertical dotted lines, is too short with respect to the alpha desynchronisation region. As a consequence, the corresponding gravity frequency  $f_g$ , drawn as a vertical solid line, is not representative of the average alpha activity related to the specific mental process. From the example, it is apparent that an individualisation of the width of the interval from  $f_1$  to  $f_2$  is required.

#### 1.1.5. Margins for improvement in IAF determination

The IAF is an intriguing concept in EEG investigation. Several methods have been proposed for IAF determination, but, as discussed above, none of them are without open issues. This explains why, among all the methods cited, the most utilised is still the simple PF method. In summary, the three major open issues are: (i) leads and band limits that are needed for the IAF computation are selected according to qualitative criteria that require visual inspection of every individual EEG spectrum, a task that can be very time consuming and difficult to reproduce from lab to lab; (ii) methods that rely on the presence of peaks in the spectra, that is, PF and EB methods, often force the user to discard data, which may represent an unacceptable loss of information; (iii) the method based on the reactivity principle, that is, the TF method, needs further refinements in the definition and individualisation of bandwidths relative to alpha activity. These three open issues call for the development of a new method that overcomes these limitations.

#### 1.2. Scope of the paper

In this article, a novel *channel reactivity based* (CRB) method is proposed for the computation of IAF in order to cope with the open issues discussed in the previous paragraph. The CRB method is designed to capture the responsiveness of alpha rhythms, regardless of the presence of peaks in the EEG spectra at rest, and to adapt the frequency intervals to individual and task specific alpha activity. This is accomplished by means of procedures based on a mathematical formalisation that allows reliance on quantitative criteria and circumvention of the need to visually inspect every individual EEG spectrum. As will be shown in the next section, the CRB method requires the setting of seven parameters, a task for which heuristic guidelines will be provided along with nominal values. Once these parameters have been set, considerable amounts of data can be quickly processed without any further user intervention and results can be precisely reproduced from lab to lab.

After a presentation of the method, the CRB method will be tested on EEG signals recorded from 19 subjects during an alternative-choice reaction time task based on a letter matching paradigm (Bisiacchi et al., 2009). Results yielded by the CRB method will be thoroughly compared with those obtained with the widely utilised PF approach. Performance of EB and TF methods on the same data will also be presented. The results will demonstrate the effectiveness of the CRB method and its capability to overcome the limits of PF, EB and TF methods. Besides, the role of the algorithm's parameters will be discussed.

## 2. Material and methods

### 2.1. EEG acquisition protocol and pre-processing

The EEG data utilised in the present study were collected from 19 subjects performing a letter matching task. The mean age was  $38 \pm 17$  (mean  $\pm$  SD) years. None of the subjects had a history of neurological/neuropsychiatric disorders or dementia; furthermore none of the subjects were taking psychotropic medications, and none had any impairment of visual acuity or colour blindness. All of the participants were seated in front of a colour monitor screen, with a fixed distance of 80 cm between their eyes and the screen. Participants were asked to evaluate five-letter strings (e.g. DFDFF) and to decide whether the letters in the second and fourth positions (relevant positions) were identical (matched condition) or not (unmatched condition). Details of the task can be found in Section 2.2.1 of Bisiacchi et al. (2009). The task consisted of eight blocks of 36 trials each (18 matched and 18 unmatched trials) and was conducted in a single session of approximately 30 min. Each trial started with a presentation of a fixation cross displayed for 800 ms. After display of a blank screen for 100 ms, the five-letter string was displayed for 1600 ms or until the participant responded, followed by a fixed blank screen for 1700 ms.

The EEG was continuously recorded from 29 Ag/AgCl electrodes mounted according to the international 10/20 system. The montage included the following scalp positions: Fp1, Fp2, F7, F3, Fz, F4, F8, FC5, FC1, FC2, FC6, T3, C3, Cz, C4, T4, CP5, CP1, CP2, CP6, T5, P3, Pz, P4, T6, PO3, PO4, O1, and O2. Fpz was used as a ground, and the reference was provided by the right and left mastoid electrodes linked together. Two electrodes were placed on the outer cantus and under the left eye to record eye movements (horizontal and vertical EOG). Each channel had its own analog-to-digital converter. The EEG and EOG signals were digitalised online with a frequency rate of 512 Hz and a conversion resolution of 0.19 mV/digit.

Offline, the signals were digitally filtered between 0.4 and 100 Hz utilising a cascade of high-pass and low-pass linear phase FIR filters. The signals were resampled at 256 Hz and were epoched into trials that spanned from  $-2$  to  $2$  s with respect to the stimulus onset. Epochs corresponding to an incorrect answer were excluded. In order to remove artefacts, data were first visually inspected to discard badly distorted epochs; then, using the infomax-based independent component analysis algorithm implemented in EEGLAB (Delorme and Makeig, 2004), artefactual components were isolated and removed from the signal (Delorme et al., 2007). The intervals from  $-2$  to  $-1$  s and from  $0$  to  $1$  s with respect to the string onset were taken as resting and test intervals, respectively. For each subject and lead, the mean resting and test spectra, denoted as  $\mathcal{R}(f)$  and  $\mathcal{T}(f)$  respectively, were obtained by averaging over the pruned epochs' single trial spectra computed during resting and test intervals, respectively. Each single trial spectrum was obtained by first multiplying the signal by a Hanning window and then applying a Fast Fourier Transform (FFT) algorithm (Stoica and Randolph, 1997).

### 2.2. The new channel reactivity based (CRB) method for IAF determination

The CRB method determines, for each subject, the IAF through the following three steps: i) definition of a reactivity index  $\rho$  and localisation of the alpha responsiveness region for each lead; ii) selection of the leads with the highest values of reactivity index; iii) determination of the IAF. These three steps are explained in the following. The reader may refer to the block diagram in Fig. 2 for a synthetic graphical illustration of the method and to Appendix A for a list of all acronyms and symbols introduced throughout the manuscript.

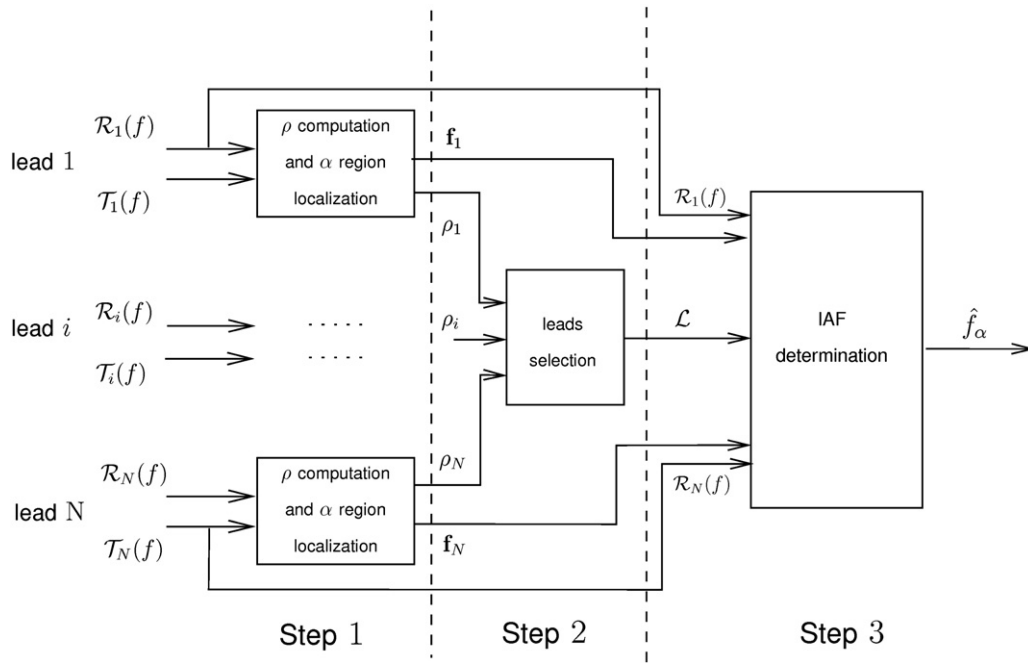


**Fig. 2.** Block diagram illustrating the three steps of the CRB method.  $\mathcal{R}_i(f)$  and  $\mathcal{T}_i(f)$  are the resting and test spectrum, respectively, for the  $i$ -th lead;  $\mathbf{f}_i = (f_1, f_2)$ , where  $f_1$  and  $f_2$  are the boundaries of the responsiveness interval for the  $i$ -th lead;  $\rho_i$  is the reactivity index relative to  $\mathbf{f}_i$ ;  $\mathcal{L}$  is the set of leads selected by the CRB method and  $\hat{f}_\alpha$  is the individual alpha frequency (IAF, determined as the median of the CAFs relative to the leads in  $\mathcal{L}$ ).

2.2.1. Step 1: definition of the reactivity index and localisation of the alpha responsiveness region

In order to quantify the responsiveness of rhythms in the alpha range, a *reactivity index*  $\rho$  is first introduced. Its utility is better understood by referring to the graphs in Fig. 3. Panels (a), (b), (c), and (d) show four examples of EEG spectra at rest. In case (a) a clear peak in

the alpha range is present, in case (b) more than one peak is detectable, and in cases (c) and (d) no clear peak can be seen. In the literature, the most common way to treat the latter three cases is by visually determining an interval to compute a gravity frequency [case (b)] or by discarding the subject's data [cases (c) and (d)]. However, if the resting spectra are superimposed on the relative test

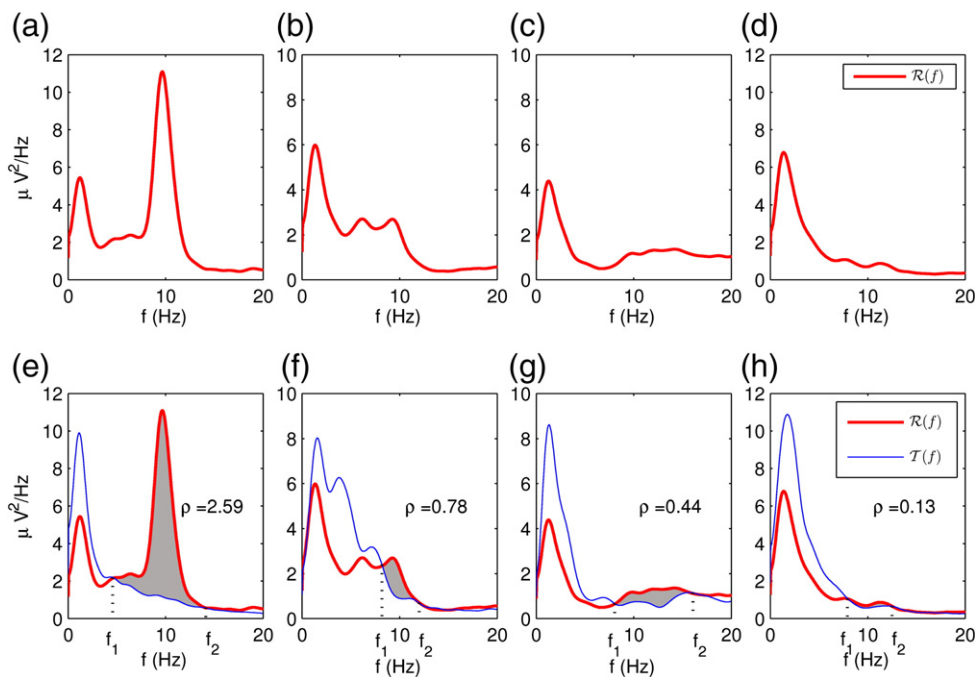


**Fig. 3.** Panels (a)–(d): four representative cases of resting EEG spectra (red). Panels (e)–(h): the same as (a)–(d) with superimposed test EEG spectra (blue) and responsiveness regions shaded in grey. The  $\rho$  values were computed using the area of the shaded region [numerator of Eq. (1)] and the frequency interval ( $f_1, f_2$ ) [denominator of Eq. (1)]. (For interpretation of the references to colour in this figure legend, the reader is referred to the web version of this article.)

spectra, new insights into the rhythms' behaviour are obtained. In fact, as graphs (e), (f), (g), and (h) of Fig. 3 illustrate, a desynchronisation region, shaded in grey, now becomes evident and also occurs for the cases that would usually have been discarded. As reported by Klimesch (1999), this kind of alpha reactivity is typical of most cognitive tasks. The scope here is to mathematically formalise this behaviour, regardless of the presence of peaks in the resting spectrum. To this aim, we quantify the rhythms' responsiveness in the frequency interval  $(f_a, f_b)$  through the reactivity index  $\rho$ , defined as

$$\rho = \mathcal{A}/(f_b - f_a), \quad (1)$$

where  $f_a$  and  $f_b$  are two frequency boundaries and  $\mathcal{A}$  is the area of the region delimited by the superimposed resting and test spectra in the interval  $f_a$  to  $f_b$ , computed as  $\int_{f_a}^{f_b} (\mathcal{R}(f) - \mathcal{T}(f)) df$ . The reactivity index is measured in  $\mu V^2/Hz$  and represents the mean responsiveness power per unit of frequency in the interval  $f_a$  to  $f_b$ . As an example,  $\rho$  values were computed for spectra in panels (e), (f), (g), and (h) of Fig. 3, utilising the frequencies  $f_1$  and  $f_2$  and the area of the shaded regions in Eq. (1). The values are reported in the figure.

The aim of the first step of the CRB method is to individuate, for each lead, the frequency interval  $(f_1, f_2)$  that delimits the whole alpha responsiveness region and to compute the relative  $\rho$  index. The frequencies  $f_1$  and  $f_2$ , for simplicity of notation, are thought to be the components of a two-dimensional vector  $\mathbf{f}$ . Accordingly, in the block diagram of Fig. 2, the frequency interval and the relative  $\rho$  value determined in Step 1 for lead  $i$  are indicated as  $\mathbf{f}_i$  and  $\rho_i$ , respectively.

In order to formalise the procedure for the determination of  $f_1$  and  $f_2$ , and to avoid qualitative choices for every subject, we developed a procedure that is capable of localising the responsiveness region through a preliminary scanning and a second expansion phase. The aim of the scanning phase is to individuate an initial interval inside the responsiveness region by scanning the frequency axis. In the second phase, this frequency interval is expanded in order to encompass the whole responsiveness region. For the sake of paper readability, the details are reported in Appendix B.

### 2.2.2. Step 2: leads selection

Reactivity indexes and alpha responsiveness intervals as determined for all leads in Step 1 are involved in the selection of leads that will participate in the computation of the subject's IAF, as illustrated by Step 2 in Fig. 2. In particular, the CRB method procedure for leads selection implements the following two principles: (i) under a minimum  $\rho$  value a lead is considered not to present any detectable alpha activity; (ii) the selection of a lead is also determined by the subject's overall alpha reactivity. The second principle is aimed at taking into account the inter-individual variability of the alpha activity that determines very different  $\rho$  values from subject to subject. Based on these two principles, the following thresholding procedure was defined. By denoting, for each subject, the whole set of  $\rho$  values as  $\{\rho_i\}_{i=1:N}$ , where  $i$  is the lead index and  $N$  the total number of leads, the set of selected leads, denoted as  $\mathcal{L}$ , is determined as

$$\mathcal{L} = \left\{ i : \rho_i > \max(\rho_{\min}, \rho_{\text{sub}}) \right\}, \quad (2)$$

where  $\max(\cdot, \cdot)$  denotes the function that selects the maximum between its arguments, and  $\rho_{\min}$  and  $\rho_{\text{sub}}$  are two thresholds defined as follows. Threshold  $\rho_{\min}$  is the minimum  $\rho$  value under which no activity is considered to be present and it is equal for all subjects. Threshold  $\rho_{\text{sub}}$  varies from subject to subject and depends on his or her individual overall reactivity. The parameter  $\rho_{\text{sub}}$  allows the discarding of leads that show a reactivity that is too low with respect to the subject's overall responsiveness and is defined as follows. Leads that exhibit some activity for the subject are those obtained

after the thresholding of his or her  $\rho$  values by  $\rho_{\min}$ . The set  $\mathcal{P} = \{\rho_i\}_{i:\rho_i > \rho_{\min}}$  contains  $\rho$  values of these leads and allows the quantification of the subject's responsiveness. In order to discard leads that show a relatively weak responsiveness, we define the fraction  $r$  of the maximum reactivity that renders a lead out of range for the subject. Accordingly, the threshold  $\rho_{\text{sub}}$  is defined as

$$\rho_{\text{sub}} = r \cdot \text{percentile}(\mathcal{P}, p), \quad (3)$$

where  $\text{percentile}(\mathcal{P}, p)$  denotes a function that computes the  $p$ -th percentile of the set  $\mathcal{P}$ .

The selection procedure is represented by the *leads selection* block in Fig. 2, whose output is the set  $\mathcal{L}$  of leads selected as in Eq. (2).

### 2.2.3. Step 3: IAF determination

The final step consists in computing the IAF for each subject. In Fig. 2, the block corresponding to Step 3 is denoted as *IAF determination* and the individual frequency is output as  $\hat{f}_\alpha$ . First, a frequency representative of its alpha activity is determined for each of the selected leads in the set  $\mathcal{L}$ . This frequency is called the channel alpha frequency (CAF) and is computed, for each lead  $i$  in  $\mathcal{L}$ , as the gravity centre of the resting spectrum  $\mathcal{R}_i(f)$  over the frequency interval  $\mathbf{f}_i$  determined in Step 1. Formally, this corresponds to

$$f_{\alpha,i} = \frac{\int_{\mathbf{f}_i} \mathcal{R}_i(f) f df}{\int_{\mathbf{f}_i} \mathcal{R}_i(f) df}, \quad i \in \mathcal{L}. \quad (4)$$

Once the CAFs for the leads in  $\mathcal{L}$  have been estimated, the IAF is determined as their median.

## 3. Results and discussion

This section is devoted to the presentation of results obtained from the 19 subjects who participated in the letter matching experiment. Even if the aim is to provide IAF estimates (the outcome of Step 3 in Fig. 2), it is also worthwhile to analyse and discuss what is obtained in the intermediate steps of the procedure. Therefore, we will first present the outcomes relative to the reactivity indexes and leads selection (Steps 1 and 2 with reference to Fig. 2). This will help in convincing the reader of the reliability of the selection procedure. Then, the results from IAF estimates (Step 3) will be thoroughly discussed and compared to those provided by the popular PF method as well as to those provided by EB and TF methods (Section 3.2). Finally, the role of user-defined CRB parameters will be discussed (Section 3.3).

### 3.1. Step 1 and Step 2 results (reactivity indexes and leads selection)

For each subject, reactivity indexes for all leads were computed as in Eq. (1), where  $f_1$  and  $f_2$  are the boundaries of the alpha responsiveness interval determined in Step 1 of CRB by applying the procedure described in Appendix B with  $w_{\text{size}} = 2$  Hz,  $w_{\text{shift}} = 0.2$  Hz,  $\lambda = 0.5$  and  $\varepsilon = 0.5$ . In order to illustrate the effectiveness of the reactivity index in quantifying the level of alpha responsiveness, panels (e), (f), (g) and (h) of Fig. 3 show four representative graphs with superimposed resting (red) and test (blue) EEG spectra, along with  $f_1$ ,  $f_2$  and  $\rho$  values. By inspecting the figure, it can be seen that  $\rho$  is higher for more accentuated alpha responses (e.g.  $\rho = 2.59 \mu V^2/Hz$  in case (e)), whereas it is lower for the less accentuated ones (e.g.  $\rho = 0.13 \mu V^2/Hz$  in case (h)).

Reactivity indexes obtained in Step 1 feed the lead selection block, the aim of which is to select the leads with the highest  $\rho$  values. The selection was carried out by applying Eq. (2), where  $\rho_{\min}$  and  $\rho_{\text{sub}}$  were set as follows. The threshold  $\rho_{\min}$  was set to  $0.15 \mu V^2/Hz$ . Accordingly, the case of panel (h), that corresponds to a  $\rho$  value of

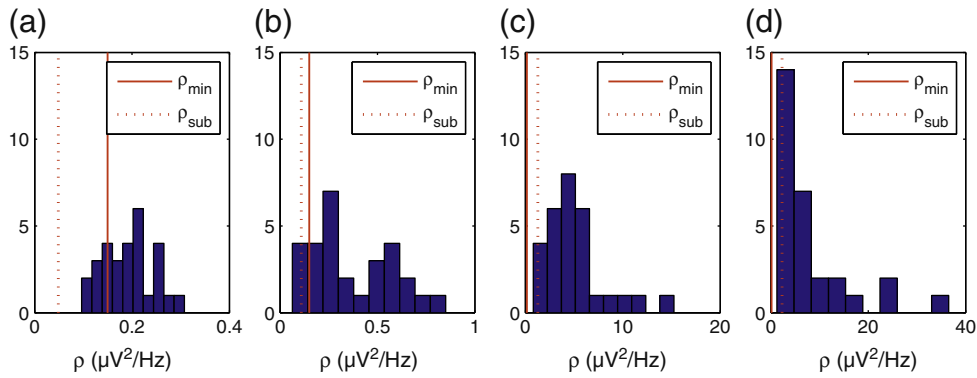


**Fig. 4.** Distribution of  $\rho$  in four representative subjects. Vertical lines are drawn in correspondence with  $\rho_{min}$  (solid red) and  $\rho_{sub}$  (dotted red). (For interpretation of the references to colour in this figure legend, the reader is referred to the web version of this article.)

0.13  $\mu V^2/Hz$ , is an example of a lead not showing significant alpha responsiveness. The threshold  $\rho_{sub}$ , that was introduced to discard the leads with an alpha activity too low with respect to the subject’s overall activity, was determined as in Eq. (3) with  $r$  and  $p$  set to 0.2 and 80, respectively. In order to show the inter-individual variability of  $\rho$  values, four representative subjects were selected and the set of  $\rho$  values computed for all their leads were represented in a histogram for each of them. The distributions of  $\rho$  values relative to the four subjects selected are reported in panels (a), (b), (c) and (d) of Fig. 4. As evident from the figure, different  $\rho$  ranges are covered by each subject, spanning from the (0.1, 0.3)  $\mu V^2/Hz$  interval of case (a) to the (1.2, 36.6)  $\mu V^2/Hz$  interval of case (d). Distributions like the one in graph (d), which show some isolated values (e.g. 34.8  $\mu V^2/Hz$ ), confirm the need of the percentile operator in Eq. (3) in order to make the definition of  $\rho_{sub}$  robust to the presence of outliers. Two vertical lines, that represent  $\rho_{min}$  (solid red) and  $\rho_{sub}$  (dotted red), are superimposed on each of the four  $\rho$  distributions in order to show some examples of how the two thresholds determine the selection of leads. In some cases  $\rho_{min}$  is more strict than  $\rho_{sub}$  (panels (a) and (b)), whereas in other cases it is the contrary (panels (c) and (d)).

The number of leads  $L$  that were selected for each subject is reported in brackets in the row of Table 1 relative to CRB. As shown in the table,  $L$  spans from 6 to 29. It is interesting to note that only four subjects out of nineteen have less than 17 selected leads. We determined that the localisation of the selected leads for these four subjects is mainly parieto-occipital. More commonly, the selected leads are distributed as shown in the topographic plot of Fig. 5, where, for each lead, the resting (red) and test (blue) spectra are superimposed on the same graph. Leads that were selected by CRB are highlighted by a grey background and the responsiveness regions that were localised at Step 1 are shaded in grey. As the figure shows, the alpha responsiveness region spans from the occipital to the frontal leads. This result is coherent with the hypothesis of an attentional fronto-parietal network involving alpha rhythms (Palva and Palva, 2007). Note that the CRB correctly selected T4 as not being an active lead, the spectra of which do not exhibit an evident alpha desynchronisation behaviour.

3.2. Step 3 results (individual alpha frequencies) and comparison with other literature methods

Individual alpha frequencies were computed for all subjects by applying both the CRB method described in Section 2.2 and the literature methods PF, EB, and TF reviewed in Section 1.

The PF method was implemented as follows. For each subject, the leads that participated in IAF computation were those selected in Step 2 of the CRB method. The method first determines the CAF as the frequency that corresponds to the highest peak of the resting spectrum in a fixed alpha frequency interval for each of these leads. Then, for each subject, the IAF is computed as the average of his or her CAFs. The alpha interval was set to (8, 13) Hz (IFSECN, 1974).

Results regarding the IAF estimates are reported in Table 1 for both methods. Each column in the table is relative to one subject. IAF estimates (in Hz) for the CRB method and the PF method, and their absolute difference are reported in the first, second, and third rows, respectively. As shown in the table, these differences span from a minimum of 0 Hz (e.g. #10 and #19) to a maximum of 3.5 Hz (#1). For some subjects the estimates produced by the two approaches are quite similar (e.g. 0.1 Hz and 0.2 Hz for #6 and #8, respectively), whereas for others they differ substantially (e.g. 3.1 Hz and 3.3 Hz for #12 and #16, respectively). In order to better quantify this evidence, subjects were divided into two groups according to the absolute value of the difference between the IAFs yielded by the two approaches: a difference lower or higher than 0.5 Hz determined the assignment of the subject to group 1 or 2, respectively. According to this criterion, almost half of the subjects (9 out of 19) were assigned to group 2; grey cells in Table 1 correspond to these subjects. In order to understand how these differences were generated, all spectra related to leads that participated in the IAFs computation were visually inspected and the correctness of the CAFs localisation was assessed. The findings are illustrated in Fig. 6. The figure contains four panels: panel (a) is representative of cases in which the two methods yielded similar results, and panels (b), (c), and (d) show spectra configurations for which the CRB method and the PF method yielded different

**Table 1**

IAF estimates (in Hz) by the CRB and PF methods and their absolute differences (one for each of the 19 subjects). The number of leads  $L$  selected by the CRB method is reported in brackets. Shaded cells correspond to subjects with IAF estimates that differ by more than 0.5 Hz.

	#1	#2	#3	#4	#5	#6	#7	#8	#9	#10	#11	#12	#13	#14	#15	#16	#17	#18	#19
CRB	14.1	10.1	10.6	10.6	9.8	8.9	10.3	11	9.8	9.9	10.6	14.9	9.5	13.1	10.1	7.5	9.8	11.6	10.1
(L)	(20)	(13)	(25)	(28)	(28)	(27)	(22)	(29)	(22)	(27)	(18)	(6)	(27)	(8)	(27)	(14)	(26)	(28)	(28)
PF	10.6	12	9.7	10.4	9.6	8.8	11.1	10.8	10.7	9.9	11.3	11.8	9.9	12.5	10.1	10.8	9.8	12	10.1
diff.	3.5	1.9	0.9	0.2	0.2	0.1	0.8	0.2	0.9	0	0.7	3.1	0.4	0.6	0	3.3	0	0.4	0

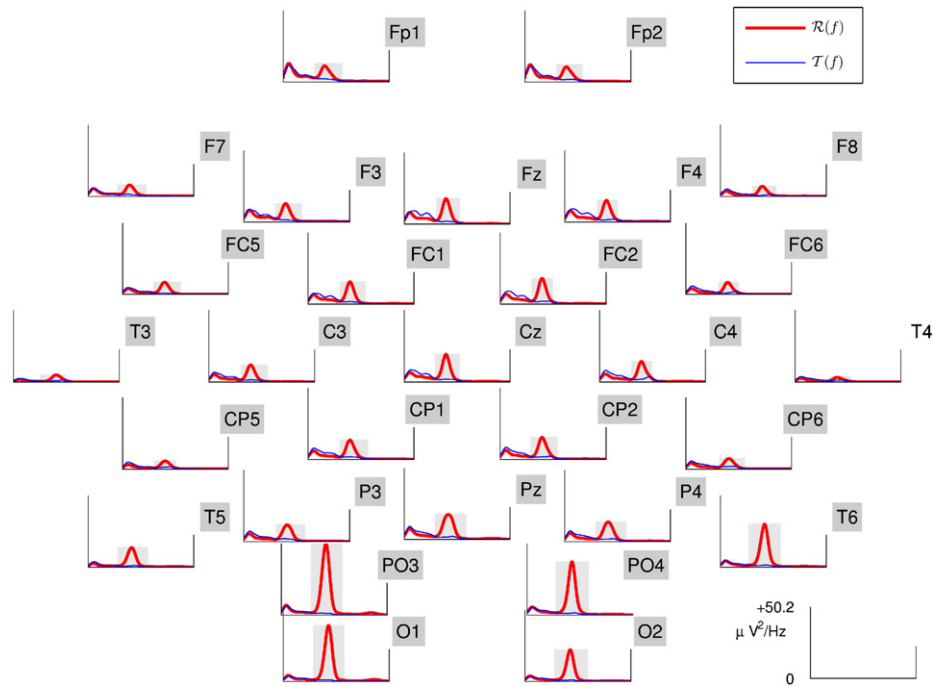


**Fig. 5.** Topographic plot of superimposed resting (red) and test (blue) EEG spectra from one representative subject. For each lead, the responsiveness regions localised by the CRB method are shaded in grey and labels of selected leads are highlighted with a grey background. (For interpretation of the references to colour in this figure legend, the reader is referred to the web version of this article.)

results. Each graph in the figure depicts superimposed resting (red) and test (blue) EEG spectra from one representative lead. CAFs determined by the CRB method and the PF method are denoted as  $f_{\alpha}$  and  $f_p$ ,

respectively, and are represented by thick and thin vertical solid lines. Responsiveness regions for CAF computation by the CRB method [Eq. (4)] are shaded in grey, and alpha ranges for CAF computation

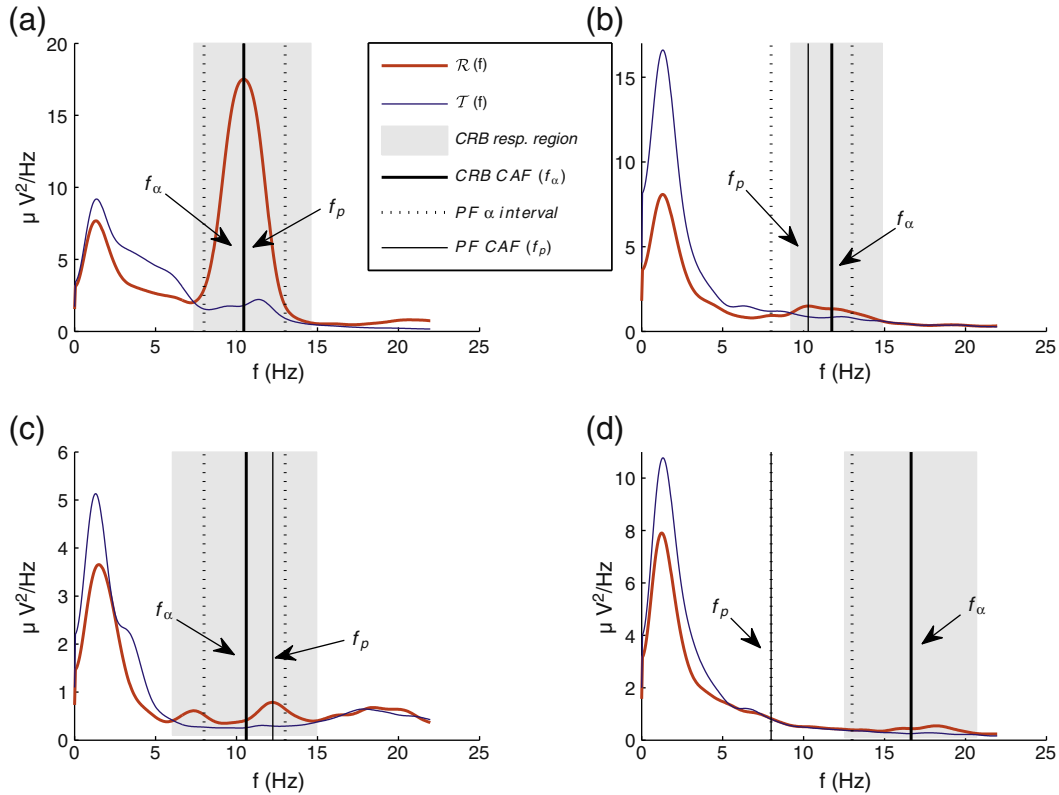


**Fig. 6.** Superimposed resting (red) and test (blue) EEG spectra corresponding to representative leads from four subjects. Panel (a) is relative to Pz and illustrates a case in which IAFs computed by the CRB method and the PF method are similar. Panels (b), (c), and (d) are relative to PO3, CP5 and Pz, respectively, and show cases in which the two IAF estimates are different. Black thick and thin vertical lines correspond to the CAFs computed by the CRB method and the PF method, respectively, which are denoted as  $f_{\alpha}$  and  $f_p$  in the graphs. Responsiveness regions localised by the CRB method are shaded in grey and the  $\alpha$  intervals for CAFs computation by the PF method are delimited by vertical dotted lines. (For interpretation of the references to colour in this figure legend, the reader is referred to the web version of this article.)

with the PF approach are delimited by two vertical dotted lines. Scales were set in order to enhance visibility. Panel (a) corresponds to one representative subject from group 1 and is relative to the lead Pz. As visible in the picture, CAFs computed with the two methods coincide and are equal to 10.4 Hz. This is determined by the fact that the resting spectrum has a clear peak in the fixed alpha range and is quite symmetric around it. Moreover, the responsiveness region corresponds to a frequency interval that is symmetric with respect to the PF. Hence, the computation of the gravity centre yields a CAF that is equal to the PF. All of the 10 subjects from group 1 had spectra configurations with similar characteristics. Pictures in panels (b), (c), and (d) correspond to each of three representative subjects from group 2 and are relative to the leads PO3, CP5, and Pz, respectively. In case (b), although the resting spectrum does not have an evident peak in the conventional alpha range, the PF method determines a CAF estimate (10.3 Hz) that corresponds to the frequency at which the resting spectrum has the highest value in the fixed alpha interval. In contrast to case (a) the responsiveness region, shaded in grey, is not symmetrical with respect to the CAF estimated by the PF method and is located at higher frequencies with respect to the fixed (8, 13) Hz interval. As the graph shows, the CAF estimated by the PF method does not seem to be representative of the channel responsiveness region. Instead, thanks to the correct localisation of the responsiveness region by the CRB method, the CAF yielded by the gravity centre operator (11.7 Hz) seems to be more representative of this specific alpha activity. Graph (c) is representative of cases in which the resting spectrum has more than one peak. In the case illustrated by the graph, the PF method detects the peak that is in the (8, 13) Hz interval, providing a CAF equal to 12.2 Hz. As the graph shows, the responsiveness region, shaded in grey, encompasses a second peak that is outside of the conventional alpha range, which is delimited by the dotted vertical lines. The CRB method correctly detects the responsiveness region and produces a CAF equal to 10.6 Hz, which is a value that takes into account the information contributed by both peaks. Panel (d) is representative of the two cases, corresponding to subjects 1 and 12, in which IAF estimates yielded by the CRB method are more than 1 Hz outside the conventional alpha range and desynchronization patterns are shifted in the beta range. In particular, in the case illustrated by this panel, the CAF yielded by PF method collapses onto the first extreme of the alpha range since  $R(f)$  has no peaks in the (8, 13) Hz interval and takes its maximum value at 8 Hz. Instead, the responsiveness region localised by the CRB method extends into the conventional  $\beta$  range and the relative CAF is representative of the desynchronisation activity that takes place in this region. All of the nine subjects from group 2 had spectra configurations similar to those reported in panels (b), (c), and (d).

**Remark.** Although in cases like that of panel (d) in Fig. 6 considering the activity individuated by the CRB method as alpha modulation may be questionable, some clues support the alpha nature of these dynamics. First, since  $\beta$  activity is mainly frontocentral, whereas  $\alpha$  is mainly posterior (Chang et al., 2010), it would be unusual to record at Pz only a beta desynchronisation without any detectable alpha desynchronisation. Moreover, as reported in the literature (Chang et al., 2010; Niedermeyer, 2005; Sanei and Chambers, 2007), it is not uncommon to see a shift of the alpha activity to higher frequencies, with peaks that can be seen in the beta range up to 20 Hz. In fact, in certain individuals an unusually fast posterior rhythm exceeds the upper limit of the alpha rhythm. Since such a rhythm shows a good blocking response to eye opening and enhancement with eye closure, it may be considered a fast equivalent of the alpha rhythm (Chang et al., 2010). Our results for subjects 1 and 12 may extend these findings in the sense that we found that there are fast rhythms that also behave equivalently to alpha rhythms during the accomplishment of a specific task.

The case studies illustrated above demonstrate that the EEG rhythmic activity varies significantly from subject to subject and

that responsiveness regions can also be identified when there are no peaks in the resting spectra. Our results show that many of these cases benefit from the new CRB approach, which is capable of adapting to the specific alpha activity characteristics of the subject. In fact, as illustrated above, in almost half of the total recordings (group 2) this flexibility was needed to localise the right CAF representative of the responsiveness regions generated by the subject's specific EEG rhythmic activity.

In order to provide the reader with an exhaustive picture of the performance of the CRB method versus literature approaches, we also implemented EB and TF methods.

The EB approach was implemented following the steps reported in Section 1. Accordingly, IAF estimates were determined only for subjects who had some leads with a resting spectrum showing a clear unique peak in the alpha range. Following this criterion, 8 out of 19 subjects were discarded and, for the others, only leads with a clear peak were selected. For 10 out of these 11 cases, the EB approach yielded IAF estimates similar to the CRB method, with absolute differences smaller than 0.5 Hz. In one case, the EB and CRB estimates were equal to 9.7 Hz and 10.6 Hz, respectively, with an absolute difference of 0.9 Hz. By resorting to the visual inspection of the subject's spectra, it was assessed that this difference was generated by the contribution given to the IAF estimate by CAFs relative to leads that were discarded by the EB method but not by the CRB method. An example of spectra relative to such leads is given in Fig. 7, where resting (red) and test (blue) spectra relative to FC5 are reported along with the IAF yielded by the EB method, denoted by  $\hat{f}_{EB}$  and represented as a thin vertical line, and the CAF yielded by the CRB method, denoted by  $f_{\alpha}$  and represented as a thick vertical line. In the same figure, the alpha responsiveness region localised by the CRB method is shaded in grey. As the figure shows, the CRB method correctly localises the  $\alpha$  responsiveness region and the value of  $f_{\alpha}$  (10.6 Hz) is roughly 1 Hz higher than  $\hat{f}_{EB}$ . It can be concluded that, when a clear unique peak is present in the alpha range of  $\mathcal{R}(f)$ , the CRB and the EB methods yield similar IAF estimates, unless leads selected only by the CRB method provide CAF values that cause the estimates to diverge. However, the number of discarded subjects may be significant (in our case larger than 40%).

For the TF method, the IAF was estimated by averaging the CAFs relative to the same leads selected by the CRB method, computed as the gravity centres of the resting spectra over the intervals from TF

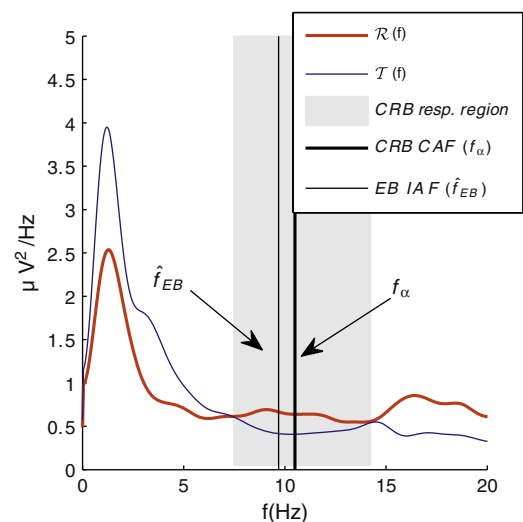


**Fig. 7.** Superimposed resting (red) and test (blue) EEG spectra relative to FC5 from a representative subject. Black thick and thin vertical lines correspond to the CAF computed by the CRB method and the IAF computed by the EB method, respectively. They are denoted as  $f_{\alpha}$  and  $\hat{f}_{EB}$  in the graph. The responsiveness region localised by the CRB is shaded in grey. (For interpretation of the references to colour in this figure legend, the reader is referred to the web version of this article.)

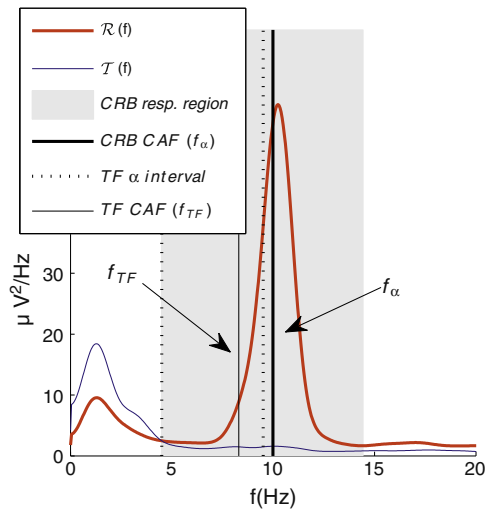


**Fig. 8.** Superimposed resting (red) and test (blue) EEG spectra relative to PO3 from a representative subject. Black thick and thin vertical lines correspond to the CAFs computed by the CRB method and the TF method, respectively. They are denoted as  $f_\alpha$  and  $f_{TF}$  in the graph. The responsiveness region localised by the CRB method is shaded in grey and the interval from TF to TF + 5 Hz for CAF computation by the TF method is delimited by two vertical dotted lines. (For interpretation of the references to colour in this figure legend, the reader is referred to the web version of this article.)

to TF + 5 Hz. The results show that, for 11 out of 19 subjects, the absolute difference between the two IAF estimates relative to the CRB method and the TF method are higher than 0.5 Hz, with values that exceed 1 Hz for seven of them. It was assessed by visual inspection that these high differences were due to the presence of alpha responsiveness regions with variable widths, for which the fixed 5 Hz bandwidth was not suitable. The example in Fig. 8 illustrates one such case. The figure plots resting (red) and test (blue) spectra relative to PO3 from one representative subject, along with CAFs determined by the CRB method and the TF method, denoted as  $f_\alpha$  and  $f_{TF}$  and represented as thick and thin vertical solid lines, respectively. In the same figure, the responsiveness region for CAF computation with the CRB is shaded grey, and the frequency interval from TF to TF + 5 Hz is delimited by two vertical dotted lines. As the figure shows, the CRB method correctly localises the responsiveness interval and  $f_\alpha$  is well representative of the frequencies involved in the  $\alpha$  activity. Instead, the interval from TF to TF + 5 Hz is too short to encompass the whole responsiveness region and the peak of  $\mathcal{R}(f)$  extends beyond the upper limit of this interval. This is the reason why  $f_{TF}$  is 1.7 Hz below  $f_\alpha$ . For this and the other 10 cases, the fixed 5 Hz bandwidth was not suitable. It can be concluded that, even when  $\mathcal{R}(f)$  shows a marked peak, a fixed alpha bandwidth may provide wrong CAFs estimates for a consistent number of subjects.

### 3.3. Role of CRB parameters

The CRB method requires the setting of seven user-defined parameters, namely,  $w_{size}$ ,  $w_{shift}$ ,  $\lambda$ ,  $\varepsilon$ ,  $\rho_{min}$ ,  $r$ , and  $p$ , of which the first four participate in Step 1, as explained in Appendix B, and the last three in Step 2, as explained in Section 2.2. In the present work they were set to 2 Hz, 0.2 Hz, 0.5, 0.5,  $0.15 \mu V^2/Hz$ , 0.2, and 80, respectively. The choice of these nominal values was driven by the role that each parameter plays in the algorithm, which is briefly summarised in the list in Appendix A for all of them. In this section, these roles will be recalled and discussed in order to provide the user with some general heuristics for setting parameter values properly. In order to investigate how variations around the parameter values chosen in this manuscript would affect the performance of the CRB method, a sensitivity analysis was carried out. For the sake of paper readability, the results are discussed in Appendix C.

The parameter  $w_{size}$  is involved in the determination of the initial frequency interval ( $f_a, f_b$ ), which is subsequently expanded to contain the whole lead's alpha responsiveness region (see also Appendix B). Hence,  $w_{size}$  should be smaller than any responsiveness region width generated by the data. The conventional alpha bandwidth is 5 Hz, but our data show that the width of the alpha responsiveness region may sometimes be smaller. By setting  $w_{size}$  equal to a small value, for example 2 or 3 Hz, these cases are taken care of and for larger responsiveness intervals the following expansion phase ensures that the initial interval is expanded to the whole region. As far as  $w_{shift}$  is concerned (see also Appendix B), the smaller its value, the more finely the frequency axis is swept. Practically, as long as  $w_{shift}$  is small enough, the potential slight approximation of  $f_a$  and  $f_b$  determined by its value does not affect the outcome of the subsequent expansion phase. Results for the sensitivity to this parameter, discussed in Appendix C, show that in our case  $w_{shift}$  could be increased up to 0.5 Hz without significantly affecting IAF estimates. The last parameter involved in the scanning phase is  $\lambda$ . As explained in Appendix B, decreasing the value of  $\lambda$  below 1 reduces the influence of a second desynchronization in the  $\beta$  range on the position of the initial interval ( $f_a, f_b$ ). At the same time, too small a value of  $\lambda$  may prevent the scanning phase from correctly identifying the complete desynchronisation interval. Once  $w_{size}$ ,  $w_{shift}$  and  $\lambda$  have been set, there are no theoretical constraints on the extent of the frequency interval to be swept. We set it to the interval (0, 40) Hz just to limit the computational burden. The fourth parameter involved in Step 1 is  $\varepsilon$ . Its role is to ensure that any local minimum of the spectrum that does not correspond to a sufficiently small difference between  $\mathcal{R}(f)$  and  $\mathcal{T}(f)$  will not be mistaken for a closure point (see also Appendix B). To achieve this,  $\varepsilon$  must be smaller than 1 and the smaller its value, the more the initial interval is expanded until  $\mathcal{R}(f)$  and  $\mathcal{T}(f)$  are sufficiently similar. However, too small a value for  $\varepsilon$  could determine the exclusion of points at which EEG spectra are close, for example  $f_2$  in Fig. B.3 (see Appendix B), from being selected as extremes of the expanded interval. As far as parameters involved in Step 2 are concerned, we recall that the threshold  $\rho_{min}$  is the minimum  $\rho$  value under which no activity is considered to be present. The smaller its value, the more leads showing scarce responsiveness will participate in the computations. Panel (h) of Fig. 3 shows an example of a lead discarded by the  $\rho_{min}$  set in this paper. The last two parameters,  $r$  and  $p$ , participate in the determination of the threshold for the discarding of leads showing too low a responsiveness with respect to the subject's overall activity [see Eq. (3)]. In particular, the  $p$ -th percentile operator, with  $p$  lower than 100, allows the computation of a value representative of the highest subject's reactivities that is not increased by outliers; and  $r$ , which takes values between 0 and 1, determines how close the reactivity of a lead must be to this representative value in order to be selected in Step 2. The higher  $r$  is, the more IAF is representative of highly responsive leads. The user may resort to the values of  $\rho$  computed by the CRB method for all leads in Step 1 to support or validate the choice of these parameters.

## 4. Conclusions

The IAF has been one of the most investigated means of characterising inter-individual variability of EEG rhythmic activity. Several methods have been proposed for IAF determination, but three main critical points of the literature methods indicate that there is still room for improvement: (i) involvement of visual inspection for the determination of each IAF and lack of quantitative criteria; (ii) requirement of peaks in the alpha range of resting spectra; (iii) lack of a fully developed procedure capable of localising rhythms actually modulated by the mental process elicited by the task. The CRB approach proposed in the present article deals with all these issues. In fact, the introduction of the reactivity index  $\rho$  and the development of the formal procedures described in Appendix B allow the detection

of task specific responsiveness regions by means of quantitative criteria, regardless of the presence of peaks in the EEG spectrum at rest. Once parameters have been set, leads are selected and CAFs and IAF are estimated without the need for visual inspection of every individual spectrum. Moreover, results can be shared in a reproducible way, and hundreds, or even thousands, of recordings from the same or similar experiments can be quickly processed without any further user intervention. A major strength of the CRB method is that it is able to deal with all the possible EEG spectra configurations, as shown in Fig. 6, and this avoids the discarding of data as occurs with the PF and EB methods when a clear peak in the alpha range is not present.

In particular, results obtained from 19 subjects on data related to a letter matching experiment showed that subjects have different levels of EEG rhythmic activity with different characteristics and topographic distributions. The CRB leads selection procedure was able to localise the leads that had the most accentuated alpha response for each subject. As far as IAF determination is concerned, while the performance of the PF, EB, and TF methods were found to be strongly dependent on EEG spectra shapes, the CRB method was seen to be much more robust. This finding suggests that the CRB method can be a good candidate for IAF determination in cases of degraded alpha response, due to recording issues or the subject's specific brain activity, age, or cerebral pathology.

It is worth noting that the CRB method, besides being a means of investigating inter-individual variability, naturally becomes an instrument for the study of intra-individual variability by focusing on CAFs instead of IAF. CAFs can be computed for all the leads with a positive reactivity index and averaged among regions of interest or utilised to compute coherence and phase locking between corresponding channels.

In order to facilitate investigations by the CRB methods, Matlab routines are at the present time in preparation as an EEGLAB (Delorme and Makeig, 2004) plugin.

To conclude, it is worth mentioning the possibility of using the CRB method on source activities obtained by independent component analysis (ICA) of recorded EEGs. In fact, ICA is widely used to linearly decompose mixed signals at scalp leads into maximally independent sources, the so-called independent components (ICs). This may allow identification of spatially distributed sources exhibiting different alpha rhythms, which, when summed at the scalp, produce multi-modal or other arbitrarily shaped spectra in the alpha range (Makeig and Onton, 2011). By applying the CRB method to ICs instead of actually recorded EEGs, the alpha rhythms of these cortical sources may be analysed individually. Reactivity indexes and frequencies analogous to CAFs may be determined for each of them and utilised to carry out several types of analysis on single sources or clusters of ICs, for example, detecting cortical sources with highly dynamic alpha activity or investigating how ICs contribute to the shaping of the spectra of the EEGs recorded from the scalp.

## Acknowledgments

Both the anonymous referees are deeply acknowledged for their thoughtful comments, suggestions, and constructive criticism. The authors are grateful to Mr. F. Parpaola for the support given in preliminary studies about the topic of the present manuscript. This work was facilitated by Cirmanmec (University of Padua) and supported by the University of Padova grant “Quantitative understanding of the human brain functioning through advanced EEG and NIRS signal processing” to GS, by the Regione Veneto FSE grants “Implementation of methodologies for the quantification of electrophysiological signals in mild cognitive disorders” to AG and “Development of a system for the analysis of the intra-individual EEG variability for the early identification of cognitive deficiencies” to CDA, and also by the Bial Foundation grant No. 146/2008 to PB.

## Appendix A. List of acronyms and symbols

Acronym	Description
CRB	Channel reactivity based
CAF	Channel alpha frequency
EB	Extended bandwidth
IAF	Individual alpha frequency
PF	Peak frequency
TF	Transition frequency
Symbol	Description
$\mathcal{D}(f)$	Difference between $\mathcal{R}(f)$ and $\mathcal{T}(f)$ (Appendix B)
$\varepsilon$	Fraction for the thresholding of $\mathcal{D}(f)$ local minima (Appendix B)
$f_1, f_2$	Boundaries of the expanded frequency interval (Appendix B)
$f_a, f_b$	Boundaries of the initial frequency interval (Appendix B)
$f_{\alpha}$	CAF yielded by the CRB method [Eq.(4)]
$f_{\alpha}$	IAF yielded by the CRB method (Step 3, Section 2.2)
$f_{EB}$	IAF yielded by the EB method (Section 3.2)
$f_g$	Centre of gravity frequency (Section 1)
$f_p$	CAF yielded by the PF method (Section 3.2)
$f_{TF}$	CAF yielded by the TF method (Section 3.2)
$\mathcal{L}$	Set of leads selected by the CRB method [Eq. (2)]
$\lambda$	Parameter for multiplicative weights computation [Eq. (B.1)]
$p$	Percentile value for the computation of $\rho_{sub}$ [Eq. (3)]
$r$	Fraction for the computation of $\rho_{sub}$ [Eq. (3)]
$\rho$	Reactivity index [Eq. (1)]
$\rho_{min}, \rho_{sub}$	Thresholds for selecting leads in the CRB method (Step 2, Section 2.2)
$\mathcal{P}$	Set of leads with $\rho$ values greater than $\rho_{min}$ (Section 2.2)
$\mathcal{R}(f)$	Resting spectrum (Section 2.1)
$\mathcal{T}(f)$	Test spectrum (Section 2.1)
$w_{shift}, w_{size}$	Shift and size of the scanning window (Appendix B)

## Appendix B. Localisation of the alpha responsiveness region

The aim of this appendix is to provide some detail on the procedure implemented for the localisation of the frequencies  $f_1$  and  $f_2$  that delimit the whole alpha responsiveness region for each lead. As anticipated in the explanation of Step 1 (Section 2.2), the procedure consists of a preliminary scanning and a second expansion phase.

The aim of the first phase is to individuate, for each lead of the subject, an initial frequency interval ( $f_a, f_b$ ) inside the responsiveness region. The procedure to achieve this is graphically explained in Fig. B.1, where representative EEG resting (red) and test (blue)

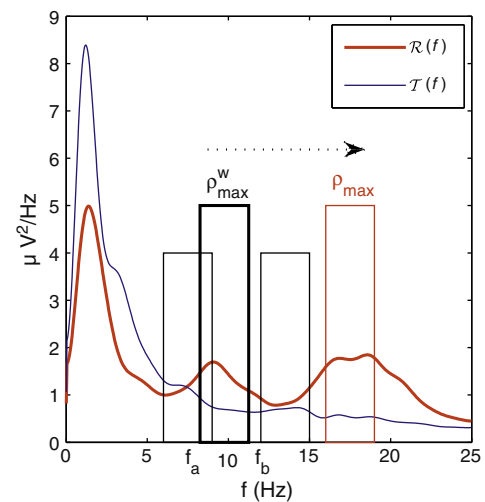


**Fig. B.1.** Scanning phase illustrated by representative resting (red) and test (blue) EEG spectra with four superimposed sliding windows. The frequencies  $f_a$  and  $f_b$  delimit the window with the highest weighted  $\rho$  value ( $\rho_{max}^w$ ), which is highlighted by a thick black rectangle. The red rectangle is drawn in correspondence with the window with the highest unweighted  $\rho$  value ( $\rho_{max}$ ). (For interpretation of the references to colour in this figure legend, the reader is referred to the web version of this article.)

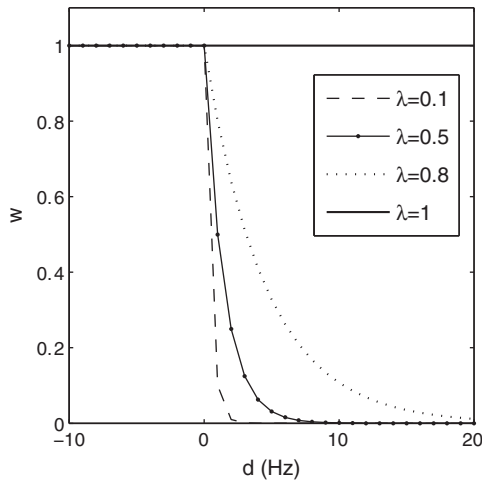


Fig. B.2. Weights ( $w$ ) versus distances ( $d$ ) for different  $\lambda$  values.

spectra are superimposed. As illustrated in the figure, the frequency axis is swept by using a window with a fixed width ( $w_{size}$ ) that is shifted by small steps ( $w_{shift}$ ), and  $\rho$  values are computed for each frequency interval individuated by the sliding window.

In order to handle cases in which a weak alpha desynchronisation is followed by a more pronounced beta modulation, as in Fig. B.1, a regularisation factor  $\lambda$  is utilised. By means of  $\lambda$ ,  $\rho$  values of windows with an upper limit greater than 13 Hz are reduced according to their distance from the conventional alpha range (8, 13) Hz. Formally, this is obtained by multiplying, for each window  $i$ , the relative  $\rho$  value by the weight

$$w_i = \begin{cases} 1, & \text{for } d_i \leq 0 \\ \lambda^{d_i}, & \text{for } d_i > 0 \end{cases} \quad (\text{B.1})$$

where  $d_i$  is the difference in Hz between the upper limit of the window and 13 Hz. The role of  $\lambda$  in determining  $w_i$  is graphically illustrated by Fig. B.2. As the figure shows,  $\lambda$  controls the rate of the exponential decay of  $w_i$  for positive distances.

By utilising the weights computed as in Eq. (B.1), reduced values, denoted by  $\rho^w$ , can be computed for all windows as

$$\rho_i^w = w_i \cdot \rho_i \quad i = 1, \dots, N_w, \quad (\text{B.2})$$

where  $N_w$  is the total number of windows. The smaller  $\lambda$  is, the more pronounced the  $\beta$  modulation must be to yield  $\rho^w$  values bigger than those relative to the windows inside the alpha responsiveness region.

The initial interval ( $f_a, f_b$ ) is determined as the one that corresponds to the window with the maximum  $\rho^w$  value ( $\rho_{max}^w$ ). The example reported in Fig. B.1 shows a case in which, by means of a regularisation factor smaller than 1, the initial interval ( $f_a, f_b$ ), highlighted by the thick black rectangle, is correctly localised inside the alpha responsiveness region. In the same example, by setting  $\lambda$  equal to 1, which is equivalent to not having any regularisation mechanism, the outcome of the scanning phase would have been the interval highlighted by the red rectangle, which corresponds to the maximum  $\rho$  value ( $\rho_{max}$ ).

The aim of the second phase is to expand the initial frequency interval ( $f_a, f_b$ ) to encompass the whole responsiveness region. In order to support the explanation, Fig. B.3 depicts an enlargement of the portion of the graph in Fig. B.1 that contains the responsiveness region. In the figure, the initial interval is marked in dark grey and its boundaries are denoted as  $f_a$  and  $f_b$ , whereas the expanded interval, corresponding to the whole responsiveness region, is marked in light grey and its boundaries are denoted as  $f_1$  and  $f_2$ . As the figure shows,  $f_1$  and  $f_2$  correspond to the closure points of a region shaped

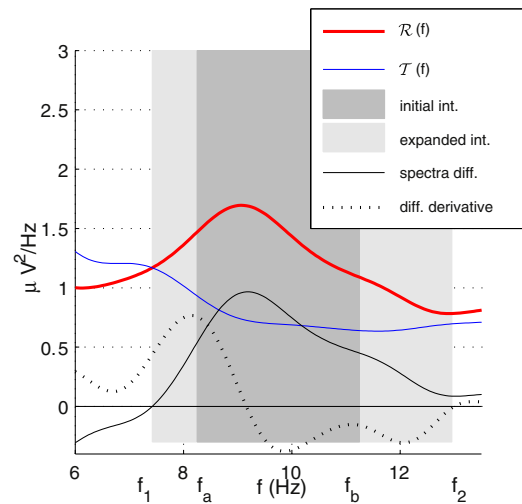


Fig. B.3. Expansion phase illustrated utilising resting (red) and test (blue) EEG spectra from a representative subject. The initial and expanded intervals are highlighted in dark and light grey, respectively. The black solid line represents the spectra difference and the dotted black line its derivative. (For interpretation of the references to colour in this figure legend, the reader is referred to the web version of this article.)

like an “eye”. In general, closure points may be frequencies at which resting and test spectra intersect, like  $f_1$  in Fig. B.3, or frequencies at which the difference between the spectra takes small values before starting to increase again, like  $f_2$ .

Closure points  $f_1$  and  $f_2$  are determined as follows. The difference spectrum  $\mathcal{D}(f) = \mathcal{R}(f) - \mathcal{T}(f)$ , for example the solid black line in Fig. B.3, is computed first. The lower limit of our expanded interval,  $f_1$ , is then determined as the highest frequency less than  $f_a$  for which  $\mathcal{D}(f)$  is equal to zero. The upper limit,  $f_2$ , is determined as the lowest frequency greater than  $f_b$  for which  $\mathcal{D}(f)$  exhibits a local minimum that is “sufficiently close” to zero. The threshold for “sufficiently close” is a pre-determined fraction  $\varepsilon$  of the maximum value of  $\mathcal{D}(f)$  over the interval ( $f_a, f_b$ ). Local minima can be identified in the typical manner by selecting zero-crossings of the first derivative of  $\mathcal{D}(f)$  for which the second derivative is positive. The example in Fig. B.3 demonstrates a case in which the initial interval (8.2, 11.2) Hz, shaded in dark grey, is expanded to the interval (7.5, 13) Hz, shaded in light grey.

## Appendix C. A sensitivity analysis

In order to investigate how the seven user-defined parameters affect CRB outcomes, a sensitivity study has been performed. Given the conceptual purpose of the study, the seven parameters were allowed to take values in a finite discrete set. In particular, IAF estimates were obtained for each combination of the following values:  $w_{size} \in (1:0.5:5)$  Hz,  $w_{shift} \in (0.1:0.1:0.5)$  Hz,  $\lambda \in (0.3:0.1:1)$ ,  $\varepsilon \in (0.1:0.05:0.5)$ ,  $\rho_{min} \in (0.03:0.02:0.19)$   $\mu\text{V}^2/\text{Hz}$ ,  $p \in (70:10:100)$ ,  $r \in (0.1:0.1:0.5)$ , where the notation ( $x_1:\Delta:x_2$ ) stands for the set of values between  $x_1$  and  $x_2$  obtained by successively incrementing each value by  $\Delta$ . In order to facilitate the analysis, the results will be presented by changing one parameter at a time. In particular, for each of the seven parameters, we determined the interval for which the resulting IAF estimates were less than 0.5 Hz apart from those already obtained with the nominal parameters recalled in Section 3.3. Results for all of the 19 subjects are reported in Table C.1. The first four rows of the table are relative to the parameters involved in Step 1. Results in the first and second rows validate the comments about the settings of  $w_{size}$  and  $w_{shift}$  given in Section 3.3. In fact, the first row shows that for 6 out of 19 subjects (i.e. #1, 4, 5, 9, 12, and 16) by enhancing  $w_{size}$  beyond 3 or 3.5 Hz, changes in IAF estimates exceed 0.5 Hz; the second row shows that, for all subjects, IAF

Table C.1

Sensitivity study. For each parameter and subject, the interval for which IAF estimates are within 0.5 Hz of those in Table 1 is reported.

	#1	#2	#3	#4	#5	#6	#7	#8	#9	#10	#11	#12	#13	#14	#15	#16	#17	#18	#19
$w_{size}$	1, 3	1, 5	1, 5	1, 3, 5	1, 3, 5	1, 5	1, 5	1, 5	1, 3, 5	1, 5	1, 5	1, 3	1, 5	1, 5	1, 5	1, 3	1, 5	1, 5	1, 5
$w_{shift}$	.1, .5	.1, .5	.1, .5	.1, .5	.1, .5	.1, .5	.1, .5	.1, .5	.1, .5	.1, .5	.1, .5	.1, .5	.1, .5	.1, .5	.1, .5	.1, .5	.1, .5	.1, .5	.1, .5
$\lambda$	.3, .7	.3, .8	.3, .8	.3, 1	.3, 1	.3, 1	.3, 1	.3, 1	.3, .7	.3, 1	.3, 1	.3, .8	.3, 1	.3, 1	.3, 1	.3, 1	.3, 1	.3, 1	.3, 1
$\varepsilon$	.4, .5	.1, .5	.3, .5	.1, .5	.1, .5	.1, .5	.3, .5	.1, .5	.4, .5	.1, .5	.1, .5	.35, .5	.1, .5	.1, .5	.1, .5	.1, .5	.1, .5	.1, .5	.1, .5
$\rho_{min}$	.09, .15	.03, .19	.03, .19	.03, .19	.03, .19	.03, .19	.03, .15	.03, .19	.03, .19	.03, .19	.03, .19	.11, .17	.03, .19	.03, .17	.03, .19	.03, .19	.03, .19	.03, .19	.03, .19
$p$	70, 100	70, 100	70, 100	70, 100	70, 100	70, 100	70, 100	70, 100	70, 100	70, 100	70, 80	70, 100	70, 90	70, 90	70, 100	70, 100	70, 90	70, 100	70, 100
$r$	.1, .3	.1, .5	.2, .5	.1, .5	.1, .5	.1, .4	.1, .5	.1, .5	.1, .5	.1, .5	.1, .5	.1, .5	.1, .5	.1, .5	.1, .5	.2, .4	.1, .5	.1, .5	.1, .5

estimates are not significantly affected by variations of  $w_{shift}$  between 0.1 and 0.5 Hz. Results in the third row are relative to  $\lambda$  and show that for five subjects (i.e. #1, 2, 3, 9, and 12) a value smaller than 1 is needed to keep the changes in IAF estimates below 0.5 Hz. These subjects have a  $\beta$  desynchronisation that is more pronounced than the one located in the alpha range, for example as in Fig. B.1, and the maximum  $\lambda$  that allows management of these five cases is 0.7. Higher values are not capable of sufficiently reducing  $\rho$  values in the  $\beta$  range for all five subjects. For the other 14 subjects, the synchronisation in the  $\alpha$  range is more pronounced than the one in the  $\beta$  range and the value of  $\lambda$  does not affect the estimates. Results in the fourth row are relative to  $\varepsilon$  and show that for 14 subjects (i.e. all but #1, 3, 7, 9 and 12), by decreasing  $\varepsilon$  to the smallest value utilised in the simulations, that is, 0.1, IAF estimates are not significantly affected. This means that at the closure points of  $\alpha$  eyes (see Appendix B for the definition of an  $\alpha$  closure point), resting and test spectra are very close or intersect. For the other five subjects (i.e. #1, 3, 7, 9, and 12) there are minimum values of  $\varepsilon$ , for example 0.3 for #3, under which IAF estimates significantly change. This means that there are closure points at which the distance between resting and test spectra exceeds the “closeness” threshold determined by such small  $\varepsilon$  values. The last three rows of the table are relative to the parameters involved in Step 2. The results in the fifth row of the table show that IAF estimates of 15 out of 19 subjects (i.e. all but #1, 7, 12, and 14) are not significantly affected by variations in  $\rho_{min}$  in the range utilised for the simulations. For these subjects, one of the following conditions is satisfied: i) variations in  $\rho_{min}$  are not perceived by the algorithm since  $\rho_{sub}$  is greater than 0.19 and determines the selection of leads as in Eq. (2); ii)  $\rho_{min}$  is greater than  $\rho_{sub}$ , but all  $\rho$  values are greater than 0.19; iii) the variation of  $\rho_{min}$  determines a small change in the number of selected leads that slightly affects the estimate of IAF. Results relative to the other four subjects (i.e. #1, 7, 12, and 14) show that  $\rho_{min}$  values between 0.11 and 0.15 are needed to keep changes in IAF estimates within 0.5 Hz for all of them. The sixth row of the table is relative to the parameter  $p$  and shows that four subjects (i.e. #11, 13, 14, and 17) require  $p$  values smaller than 100 to yield IAF estimates close to those reported in Table 1. In these cases the sets of  $\rho$  values include outliers that significantly affect the value of  $\rho_{sub}$  [see Eq. (3)]. For three of these subjects (i.e. #13, 14, and 17) values from 70 to 90 yield similar IAF estimates, whereas for subject 11 the 80th percentile should not be exceeded. The last row of the table is relative to  $r$ . Results show that for 15 subjects (i.e. all but #1, 3, 6 and 16) the variation of  $r$  between values from 0.1 to 0.5 does not cause significant changes in IAF estimates. This happens when the variance of the set of CAFs is such that  $\rho_{sub}$  values relative to these  $r$  [see Eq. (3)] do not significantly affect the number of leads discarded. Results from the other four subjects (i.e. #1, 3, 6, and 16) show that  $r$  values between 0.2 and 0.3 yield IAF estimates similar to those in Table 1 in all cases.

From the discussion above, it can be concluded that once  $w_{size}$  and  $w_{shift}$  have been set to small values the fine tuning of each of the other five parameters affects only a minor number of subjects, that is five

for  $\lambda$  and  $\varepsilon$  and four for  $\rho_{min}$ ,  $p$ , and  $r$ . In these cases, there is often room for slight variations that do not significantly affect the IAF estimates.

## References

- Babiloni, C., Miniussi, C., Babiloni, F., Carducci, F., Cincotti, F., Del Percio, C., Sirello, G., Fracassi, C., Nobre, A.C., Rossini, P.M., 2004. Sub-second temporal attention modulates alpha rhythms. A high-resolution EEG study. *J. Neurosci. Methods* 19, 259–268.
- Babiloni, C., Capotosto, P., Del Percio, C., Babiloni, F., Petrini, L., Buttiglione, M., Cibelli, G., Marusiak, J., Romani, G.L., Arendt-Nielsen, L., Rossini, P.M., 2010. Sensorimotor interaction between somatosensory painful stimuli and motor sequences affects both anticipatory alpha rhythms and behavior as a function of the event side. *Brain Res. Bull.* 81, 398–405.
- Başar, E., Schürmann, M., Başar-Eroglu, C., Karakaş, S., 1997. Alpha oscillations in brain functioning: an integrative theory. *Int. J. Psychophysiol.* 26, 5–29.
- Berger, H., 1929. Über das elektroencephalogramm des menschen. *Eur. Arch. Psychiatry Clin. Neurosci.* 87, 527–570.
- Bisiacchi, P.S., Schiff, S., Ciccola, A., Kliegel, M., 2009. The role of dual-task and task-switch in prospective memory: behavioural data and neural correlates. *Neuropsychologia* 47, 1362–1373.
- Capotosto, P., Perrucci, M.G., Brunetti, M., Del Gratta, C., Doppelmayr, M., Grabner, R.H., Klimesch, W., Neubauer, A., Neuper, C., Pfurtscheller, G., Romani, G.L., Babiloni, C., 2009. Is there “neural efficiency” during the processing of visuo-spatial information in male humans? An EEG study. *Behav. Brain Res.* 205, 468–474.
- Chang, B.S., Schomer, D.L., Niedermeyer, E., 2010. Normal EEG and sleep: adults and elderly. In: Schomer, D.L., da Silva, F.H.L. (Eds.), *Niedermeyer’s Electroencephalography: Basic Principles, Clinical Applications, and Related Fields*, 6th Edition. Lippincott Williams & Wilkins, Baltimore, MD, pp. 183–214.
- Clarka, C.R., Veltmeyer, M.D., Hamilton, R.J., Simms, E., Paul, R., Hermens, D., Gordon, E., 2004. Spontaneous alpha peak frequency predicts working memory performance across the age span. *Int. J. Psychophysiol.* 53, 1–9.
- Coben, L., Danziger, W., Storandt, M., 1985. A longitudinal EEG study of mild senile dementia of Alzheimer type: changes at 1 year and at 2.5 years. *Electroencephalogr. Clin. Neurophysiol.* 61, 101–112.
- Delorme, A., Makeig, S., 2004. EEGLAB: an open source toolbox for analysis of single-trial EEG dynamics including independent component analysis. *J. Neurosci. Methods* 134, 9–21.
- Delorme, A., Sejnowski, T., Makeig, S., 2007. Enhanced detection of artifacts in EEG data using higher-order statistics and independent component analysis. *Neuroimage* 34, 1443–1449.
- Doppelmayr, M., Klimesch, W., Pachinger, T., Ripper, B., 1998. Individual differences in brain dynamics: important implications for the calculation of event-related band power. *Biol. Cybern.* 79, 49–57.
- Doppelmayr, M., Klimesch, W., Hödlmoser, K., Sauseng, P., Gruber, W., 2005. Intelligence related upper alpha desynchronization in a semantic memory task. *Brain Res. Bull.* 66, 171–177.
- Epstein, H.T., 1980. EEG developmental stages. *Dev. Psychobiol.* 13, 629–631.
- Gevens, A., Smith, M.E., McEvoy, L., Yu, D., 1997. High-resolution EEG mapping of cortical activation related to working memory: effects of task difficulty, type of processing, and practice. *Cereb. Cortex* 7, 374–385.
- Grabner, R.H., Brunner, C., Leeb, R., Neuper, C., Pfurtscheller, G., 2007. Event-related EEG theta and alpha band oscillatory responses during language translation. *Brain Res. Bull.* 72, 57–65.
- Hadley, J., 1941. Some relationship between electrical signs of central and peripheral activity during “mental work”. *J. Exp. Psychol.* 28, 53–62.
- IFSECN, 1974. A glossary of terms commonly used by clinical electroencephalographers. *Electroencephalogr. Clin. Neurophysiol.* 37, 538–548.
- Klimesch, W., 1997. EEG alpha rhythms and memory processes. *Int. J. Psychophysiol.* 26, 319–340.
- Klimesch, W., 1999. EEG alpha and theta oscillations reflect cognitive and memory performance: a review and analysis. *Brain Res. Rev.* 29, 169–195.
- Klimesch, W., Schimke, H., Ladumer, G., Pfurtscheller, G., 1990. Alpha frequency and memory performance. *J. Psychophysiol.* 4, 381–390.
- Klimesch, W., Schimke, H., Pfurtscheller, G., 1993. Alpha frequency, cognitive load and memory performance. *Brain Topogr.* 5, 241–251.

- Klimesch, W., Doppelmayr, M., Russegger, H., Pachinger, T., 1996. Theta band power in the human scalp EEG and the encoding of new information. *Neuroreport* 7, 1235–1240.
- Klimesch, W., Doppelmayr, M., Schimke, H., Ripper, B., 1997. Theta synchronization and alpha desynchronization in a memory task. *Psychophysiology* 34, 169–176.
- Klimesch, W., Vogt, F., Doppelmayr, M., 2000. Interindividual differences in alpha and theta power reflect memory performance. *Intelligence* 27, 347–362.
- Klimesch, W., Schack, B., Schabus, M., Doppelmayr, M., Gruber, W., Sauseng, P., 2004. Phase-locked alpha and theta oscillations generate the P-N1 complex and are related to memory performance. *Cogn. Brain Res.* 19, 302–316.
- Knott, J., 1938. Brain potentials during silent and oral reading. *J. Gen. Psychol.* 18, 57–62.
- Koch, S.P., Koendgen, S., Bourayou, R., Steinbrink, J., Obrig, H., 2008. Individual alpha-frequency correlates with amplitude of visual evoked potential and hemodynamic response. *Neuroimage* 41, 233–242.
- Köpruner, V., Pfurtscheller, G., Auer, L.M., 1984. Quantitative EEG in normals and in patients with cerebral ischemia. *Prog. Brain Res.* 62, 29–50.
- Lopes da Silva, F., 1992. The rhythmic slow activity (theta) of the limbic cortex: an oscillation in search of a function. In: Basar, E., Bullock, T. (Eds.), *Induced Rhythms in the Brain*. Birkhäuser, Boston, MA, pp. 83–1021.
- Makeig, S., Onton, J., 2011. ERP features and EEG dynamics: an ICA perspective. In: Luck, S.J., Kappenman, E.S. (Eds.), *The Oxford Handbook of Event-Related Potential Components*, 5th edition. Oxford University Press, New York, NY.
- Niedermeyer, E., 2005. The normal EEG of the waking adult. In: Niedermeyer, E., da Silva, F.L. (Eds.), *Electroencephalography. Basic Principles, Clinical Applications and Related Fields*, 5th edition. Lippincott Williams & Wilkins, Baltimore, MD, pp. 167–192.
- Nunez, P., Reid, L., Bickford, R.G., 1978. The relationship of headsize to alpha frequency with implications to a brain wave model. *Electroencephalogr. Clin. Neurophysiol.* 44, 344–352.
- Osaka, M., 1984. Peak alpha frequency of EEG during a mental task: task difficulty and hemispheric differences. *Psychophysiology* 21, 101–105.
- Palva, S., Palva, J.M., 2007. New vistas for alpha-frequency band oscillations. *Trends Neurosci.* 30, 150–158.
- Petersén, I., Eeg-Olofsson, O., 1971. The development of the electroencephalogram in normal children from the age of 1 through 15 years – non-paroxysmal activity. *Neuropadiatrie* 2, 375–404.
- Pfurtscheller, G., Lopes da Silva, F., 1999. Event-related EEG/MEG synchronization and desynchronization: basic principles. *Clin. Neurophysiol.* 110, 1842–1857.
- Raghavachari, S., Kahana, M.J., Rizzuto, D.S., Caplan, J.B., Kirschen, M.P., Bourgeois, B., Madsen, J.R., Lisman, J.E., 2001. Gating of human theta oscillations by a working memory task. *J. Neurosci.* 21, 3175–3183.
- Rugg, M.D., Dickens, A.M., 1982. Dissociation of alpha and theta activity as a function of verbal and visuo-spatial tasks. *Electroencephalogr. Clin. Neurophysiol.* 53, 201–207.
- Saletu, B., Grünberger, J., 1985. Memory dysfunction and vigilance: neurophysiological and psychopharmacological aspects. *Ann. N. Y. Acad. Sci.* 444, 406–427.
- Sanei, S., Chambers, J.A., 2007. *EEG Signal Processing*. John Wiley & Sons, Ltd., Chichester, England.
- Schacter, D., 1977. EEG theta waves and psychological phenomena: a review and analysis. *Biol. Psychol.* 5, 47–82.
- Smit, C.M., Wright, M.J., Hansell, N.K., Geffen, G.M., Martin, N.G., 2006. Genetic variation of individual alpha frequency (IAF) and alpha power in a large adolescent twin sample. *Int. J. Psychophysiol.* 61, 235–243.
- Stoica, P., Randolph, L.M., 1997. *Introduction to Spectral Analysis*. Prentice Hall, Upper Saddle River, NJ.